Temperature sintering effects on the magnetic, electrical and transport properties of $La_{0.67}Sr_{0.33}MnO_3/Nd_{0.67}Sr_{0.33}MnO_3$ composites

2004 J. Phys.: Condens. Matter 16 3711

(http://iopscience.iop.org/0953-8984/16/21/019)

INSTITUTE OF PHYSICS PUBLISHING JOURNAL OF PHYSICS: CONDENSED MATTER

J. Phys.: Condens. Matter **16** (2004) 3711–3718 PII: S0953-8984(04)73756-X

Temperature sintering effects on the magnetic, electrical and transport properties of $La_{0.67}Sr_{0.33}MnO_3/Nd_{0.67}Sr_{0.33}MnO_3$ composites

Y L Chang and C K Ong

Department of Physics, National University of Singapore, 10 Kent Ridge Cresent, 119260, Singapore

Received 22 December 2003
Published 14 May 2004
Online at stacks.iop.org/JPhysCM/16/3711
DOI: 10.1088/0953-8984/16/21/019

Abstract

The microstructure, magnetic and electrical transport properties of $La_{0.67}Sr_{0.33}MnO_3/Nd_{0.67}Sr_{0.33}MnO_3$ composites are studied as a function of sintering temperature. At 900 °C, the intergrain exchange couplings between the adjacent particles give rise to an increase in resistance. Raising the sintering temperature induces the formation of an interfacial phase near the $La_{0.67}Sr_{0.33}MnO_3$ and $Nd_{0.67}Sr_{0.33}MnO_3$ grain boundaries as indicated in the XRD pattern and SEM image. At 1100 °C, the formation of interfacial phases near the grain boundaries enhances the conductivity in the composite. Broad magnetoresistance across room temperature is observed in a composite sintered at 1300 °C. This observation may be ascribed to the coexistence of multiphase in the composite which leads to a decrease in resistance. The results suggest that sintering temperature has a prominent effect on the properties of the grain boundary, which plays an important role in determining the electrical transport behaviour of the composites.

1. Introduction

The large change in electrical resistance upon the application of an external magnetic field (also known as magnetoresistance, MR effect) has widely been observed in ferromagnetic metal [1–3], heterogeneous magnetic alloy [4] and manganite [5, 6] systems. The magnetoresistance (MR) effect can be separated into two parts which consist of intrinsic *intra*granular and non-intrinsic *inter*granular effects. Examples of the former include anisotropic magnetoresistance (AMR) of permalloy [7] or the colossal magnetoresistance (CMR) of EuO [8] and mixed-valence manganites [5, 6] of the perovskite-structure ABO_3. Examples of the latter are the giant magnetoresistance (GMR) of magnetic bimetallic and multimetallic layers in Fe–Cr or Co–Cu [9, 10] and ferromagnetic granules dispersed in paramagnetic metal films [11, 12]. The intrinsic intragranular MR effect that is observed in the manganite system can be tuned

by doping either at the A or B sites [13, 14]. It was usually observed under high field within a narrow temperature range near the vicinity of the magnetic transition temperature. On the other hand, it was proposed that the intergranular effect that responds to low field was attributed to the spin polarized transportation of conduction electrons between grains [13, 15]. It is this mechanism that plays a major part in potential field-sensor and magnetic recording device applications. In order to have a better understanding and control of this mechanism, a number of research groups have come up with elegant and useful experiments to understand the origins of the MR effects. A direct study of the properties of grain boundaries on the MR effects has been done by growing well-controlled $La_{2/3}Sr_{1/3}MnO_3$ (LSMO) films on bicrystalline $SrTiO_3$ substrates at various specific angles [16]. The study has conclusively shown that MR was related to the interfaces created at the bicrystal junction. Hwang *et al* [13] have also demonstrated that the observed MR at low field in $La_{2/3}Sr_{1/3}MnO_3$ was due to spin-dependent tunnelling between grains. Other observation of magnetoresistance in tunnelling-type structures, such as heterogeneous magnetic alloys with ferromagnetic grains embedded in an immiscible insulating matrix such as Ni/SiO_2 and Co/SiO_2 [17] have provided further evidence of the manifestation of conduction electrons spin-dependent scattering dependence on the local magnetic configuration. The macroscopic properties of metal–insulator mixtures depend on the variable metallic volume fraction x. At low x values, metallic grains are isolated from each other and an electric transport is realized by intergranular tunnelling or temperature activated hopping. When the metal concentration is increased above a certain threshold, individual grains form an infinite cluster with a continuous metallic conductance path. Besides the examples given above, MR can also be enhanced with high spin polarized, half-metallic FM (ferromagnetic) manganite material. It is found to be the best candidate for maximizing spin-polarization dependent devices due to the unique nature of double exchange mediated ferromagnetism results in completely polarized conduction electrons in the FM state. Examples of such granular ferromagnetic manganite combinations have already been reported in $La_{0.67}Sr_{0.33}MnO_3/CeO_2$ [18], $La_{0.7}Ca_{0.3}MnO_3$–Ag [19], $La_{0.7}Sr_{0.3}MnO_3$–$Pr_{0.5}Sr_{0.5}MnO_3$ [20] and $La_{0.67}Ca_{0.33}MnO_3$–Al_2O_3 [21] composites. The incorporation of a second phase, usually a nonmagnetic or an antiferromagnetic (AFM) insulator (I) into the FM manganite matrix can modify the magnetic scattering and hence the electron tunnelling probability at the grain boundaries.

In this paper, we report the results of the microstructure, magnetic and electrotransport properties of a composite system, which consists of two half-metallic ferromagnetic manganese oxides, $La_{0.67}Sr_{0.33}MnO_3$ (LSMO) and $Nd_{0.67}Sr_{0.33}MnO_3$ (NSMO). Here, instead of using FM/I type composites, a double soft ferromagnetic metal (FMM), FM/FM type composite was synthesized. In order to elucidate the relative importance of grain boundary in respect of the electrical transport properties, a comparative study was carried out varying the sintering temperature of the composite while keeping the doping concentration of the second phase constant. By doing this, we hope to see an improved temperature dependant of MR, especially near room temperature. Early criticisms about the technological relevance of the manganites were the fact that the field induced MR was limited to a narrow temperature range and the rapid decrease of MR with increasing temperature make them unacceptable for any real field sensing device. Optimal conditions for achieving broad CMR responses across room temperature by tuning the sintering temperature of a composite were observed and reported here and it can be viewed as a promising route that may lead to technologically important advances. LSMO and NSMO with Curie temperatures, $T_c = 380$ and 270 K, respectively, are used. The measured magnetic moment of LSMO is 3.67 μ_B/fu [22] while that of NSMO is 4.2 μ_B/fu [23] at 5 K. The coercivities of LSMO and NSMO from the measured M–H hysteresis at 78 K are $H_{cLSMO} \approx 80$ Oe and $H_{cNSMO} \approx 350$ Oe, respectively. With the combination of these

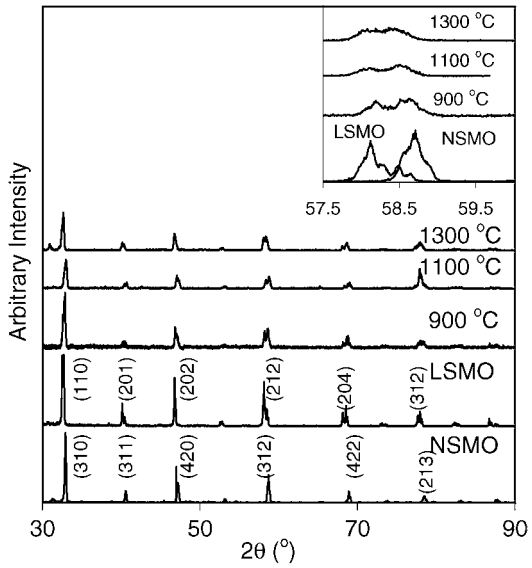

Figure 1. XRD patterns for NSMO, LSMO and a series of composites at different sintering temperatures, $T_s = 900$, 1100 and 1300 °C. The inset gives the selected range of $57° \leqslant 2\theta \leqslant 60°$ for the above five samples.

materials, no increase in resistivity to a few orders of magnitude of the composites is observed as was reported by other FM/I type synthesized composites. A high resistivity is known to make the application of the materials incompatible for practical devices.

2. Experiments

$La_{0.67}Sr_{0.33}MnO_3/Nd_{0.67}Sr_{0.33}MnO_3$ (LSMO/NSMO) composites were prepared by two steps. First, NSMO and LSMO powders were prepared by a solid-state reaction method. The detailed preparation process was described in our previous work [23]. The obtained products were then mixed in equal weight ratio and carefully ground in an agate mortar. Next, the mixed powders were pressed into pellets and finally calcined for 5 h in air at three different sintering temperatures, $T_s = 900$, 1100 and 1300 °C to achieve the desired compositions. All samples were made from the same batch and of the same dimensions from the same die. The sample phases were determined by a fine-step-mode x-ray diffraction (XRD), model Phillips Diffractometer with Cu Kα source. High-resolution scanning electron microscopy (SEM) equipped with energy dispersive x-ray analysis (EDX) has been employed to check the crystallinity, microstructures and constitution of the samples. An Oxford superconducting vibrating sample magnetometer (VSM) and a standard four-pad technique were used to evaluate the magnetic property and electrical resistivity with and without external magnetic field, H, of the samples.

3. Experimental results and discussions

Figure 1 shows the XRD patterns of LSMO, NSMO and a series of LSMO/NSMO composites at different sintering temperatures, $T_s = 900$, 1100 and 1300 °C. LSMO and NSMO samples are polycrystalline without any preferred orientation and the sintering temperature is sufficiently high to obtain a single-phase perovskite. All of the reflections lines for the parent LSMO and NSMO samples are successfully indexed with an orthorhombic structure (space group $Pnma$) ABO_3-type distorted perovskite structure. For the LSMO/NSMO composites, the diffraction peaks caused by the individual parent samples are indistinguishable from each other. Thus,

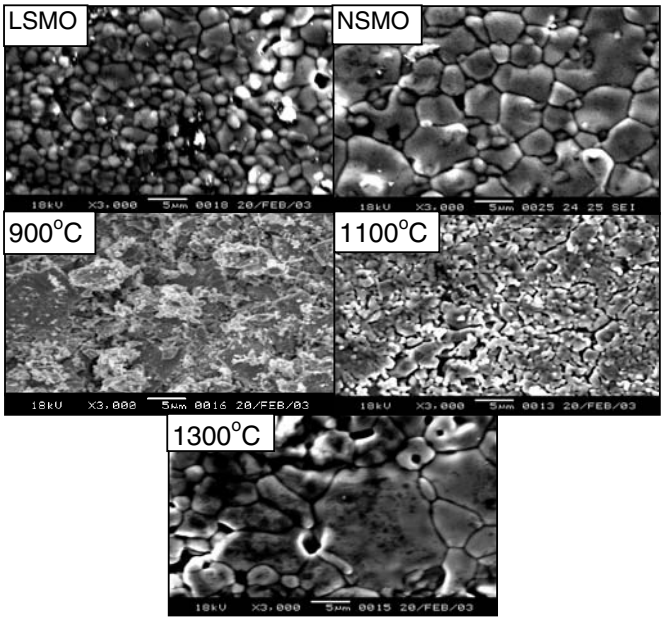

Figure 2. SEM morphologies of NSMO, LSMO and LSMO/NSMO composites of $T_s = 900$, 1100 and 1300 °C.

an inset which shows the selected range of $57° \leqslant 2\theta \leqslant 60°$ has been included. As seen in figure 1, the peak for the composite sintered at 900 °C is well represented by combination of LSMO and NSMO. It can be interpreted as having two phases of LSMO and NSMO coexisting in the composite. Upon increasing the sintering temperature up to 1300 °C, the individual peaks of LSMO and NSMO coalesce and broaden. To further confirm the dependence of sintering temperature on the microstructure, the surface morphologies of LSMO, NSMO and LSMO/NSMO composites at $T_s = 900$, 1100 and 1300 °C have been imaged by high-resolution scanning electron microscopy (SEM). As can be seen in figure 2, LSMO has smaller grains than NSMO. The average grain size for LSMO is in the range of 1–5 μm while that of NSMO is 5–10 μm. The SEM image for composite sintered at $T_s = 900$ °C shows that larger NSMO particles are well separated by smaller LSMO grains. When the composite was sintered at 1100 °C, the LSMO and NSMO particles do not seem to connect tightly, deferring from their parent samples. At $T_s = 1300$ °C, the composite has well-formed granular crystallites with grain size comparable or larger than the parent samples. By looking at the SEM images, we do not exclude the possibility that high temperature sintering helps to promote the growth of the intermediate phase of $La_{0.67(1-x)}Nd_{0.67x}Sr_{0.33}MnO_3$ in the composite due to the interfacial diffusion reaction between the LSMO and NSMO grain boundaries.

Figure 3 presents the temperature dependence of magnetization, $M(T)$ at $H = 200$ Oe for LSMO, NSMO and LSMO/NSMO composites of $T_s = 900$, 1100 and 1300 °C. As is seen, pure LSMO is in the FM state over the whole measured temperature range while pure NSMO begins to transit from paramagnetic to FM at T_c (defined as the temperature where $dM(T)/dT$ is a minimum) ≈270 K. The composites of $T_s = 900$ and 1100 °C exhibit two distinct transitions originating from NSMO and LSMO samples. At $T_s = 1300$ °C, the macroscopic magnetization curve revealed the replacement of NSMO by an additional phase with $T_c \approx 320$ K, as shown in the inset to figure 3, besides its parent LSMO and NSMO samples. From the VSM data, we can conclude that high temperature sintering in the composite of $T_s = 1300$ °C brings about the

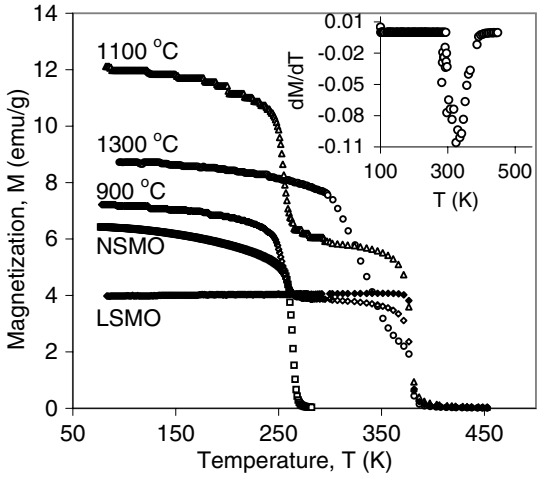

Figure 3. Temperature dependence of magnetization, $M(T)$, for NSMO, LSMO and LSMO/NSMO composites at different T_s of 900, 1100 and 1300 °C. The inset shows the temperature dependence of dM/dT for composites sintered at $T_s = 1300$ °C.

formation of a $(La_{1-x}Nd_x)_{0.67}Sr_{0.33}MnO_3$ phase as the magnetization curve revealz the gradual diminishing phase of its parent LSMO and NSMO samples. Our result was further compared with the polycrystalline sample $(La_{1-x}Nd_x)_{0.7}Sr_{0.3}MnO_3$ as reported by Wenbin *et al* [24]. According to Wenbin *et al*, the bulk samples with $x = 0.25-0.5$ prepared under similar method and conditions have transition temperatures at around 310–340 K. These seem to be consistent with our results reported above, indicating the existence of a $(La_{1-x}Nd_x)_{0.7}Sr_{0.3}MnO_3$ phase in high sintered composites.

In order to get a better insight into the enhanced boundary effect caused by the interfacial phase, the field dependence of magnetization, $M(H)$ for typical samples with LSMO, NSMO and LSMO/NSMO composites of $T_s = 900$, 1100 and 1300 °C was measured at 78 K. It is obvious that there is a distinct difference in the magnitude of magnetization of the composites as shown in figure 4. The composites of $T_s = 1100$ and 1300 °C have magnetization greater than their parent samples. The solid curve shows the as-calculated $M(H)$ for LSMO/NSMO composite according to the magnetization of the parent LSMO and NSMO weight fractions in the composite and is inserted for comparison. The experimental curve for a composite at $T_s = 900$ °C is very similar to the as-calculated $M(H)$ curve except the latter is higher in magnetization than the former. The enhanced spin disorders at the grain boundary interfaces act as extra energy barriers for the field to overcome in order to align the disorder Mn spins along the field direction. Assuming that at 78 K, though both NSMO and LSMO layers in $T_s = 900$ °C are in the FM state and no interdiffusion occurs across the LSMO and NSMO grain boundaries, however, some spins near and inside the LSMO and NSMO boundary layers may still be disorientated, resulting in a more random distribution of grain magnetization. Figure 4 shows also the field dependence of magnetic moments per formula unit at 78 K. The LSMO sample has a value of M close to the theoretical limit ($\sim 3.67\ \mu_B$) based on spin-only contributions from all Mn ions. However, the magnetic moment of NSMO reaches only $3.4\ \mu_B$ at 6 T. This shows that at 78 K, some of the Mn and Nd spins in the NSMO sample do not align ferromagnetically with each other. As a small field is applied, most spins realign themselves readily parallel to each other where the overall spins in the near boundary layers tend to point in the same direction. Hence the embedding of LSMO into NSMO particles introduces additional magnetic disorder at the grain boundary layers, leading to lower magnetization than the as-calculated $M(H)$ curve. It is observed that composite of $T_s = 1100$ °C has the highest magnetization among the three composites. This is because at $T_s = 1100$ °C the composite

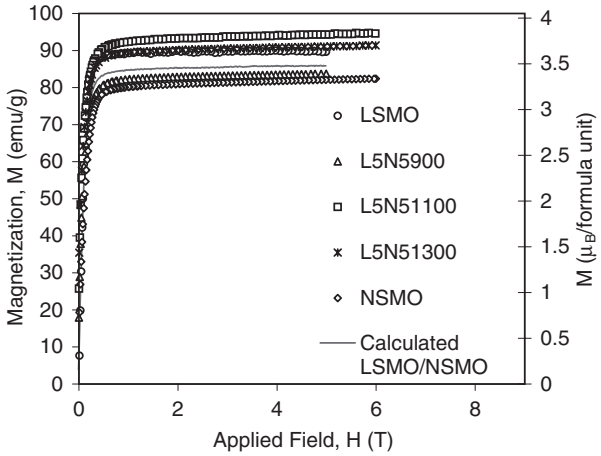

Figure 4. Field dependence of magnetization, $M(T)$, and the secondary axis shows the field dependence of magnetic moments per unit formula for NSMO, LSMO and LSMO/NSMO composites at different T_s of 900, 1100 and 1300 °C. The solid curve represents the calculated $M(H)$ according to the weight fraction of LSMO and NSMO if no interaction reaction occurs between them.

is in weaker connectivity than the composite of $T_s = 1300$ °C, resulting in the easier overall magnetic domain rotation. The result coincides with the $M(T)$ curve seen in figure 3 even when the magnetic field is still low. Based on figure 4, we can conclude the presence of interfacial diffusion between the LSMO and NSMO grains in composites with $T_s = 1100$ and 1300 °C. The higher magnetization values for composites with $T_s = 1100$ and 1300 °C than their parents and composite of $T_s = 900$ °C samples, as seen in figure 4, were attributed to interfacial diffusion across the grain boundaries during sample sintering, in addition to the contribution from non-parallel spin coupling. Thus, the interfacial diffusion reaction has induced the formation of a $(La_{1-x}Nd_x)_{0.67}Sr_{0.33}MnO_3$ phase near the grain boundaries as seen in the SEM image. This phase should be in the FMM state as shown in the inset to figure 3. Hence, it will be easier to align the spins along the field direction giving rise to higher magnetization value. At $T_s = 1300$ °C, however, the composite appears to be dominated by a $(La_{1-x}Nd_x)_{0.67}Sr_{0.33}MnO_3$ phase. Thus, the magnetization curve displays properties intrinsic to this phase. Therefore, the growth of an interfacial phase near grain boundaries and the coexistence of multiphase due to high sintering temperature have a direct effect on the microstructure and magnetic properties in these composites.

Figures 5 and 6 show the temperature dependent resistivity and MR curves at $H = 0$ and 10 kOe applied field for all samples. Here, MR is defined as $\Delta\rho/\rho_0$, where $\Delta\rho = (\rho_H - \rho_0)$ and ρ_0 and ρ_H are the resistivity at $H = 0$ and 10 kOe, respectively. At $T_s = 900$ °C, the composite has an insulator–metal transition temperature, $T_p \approx 268$ K, originating primarily from its parent NSMO component. This result further confirms the hypothesis made earlier that two phases from its parent samples coexist in the lowest T_s composite. Composites of $T_s = 1100$ and 1300 °C exhibit lower $T_p \approx 255$ K and the resistivity continues to increase with increasing temperature unlike those from its parents and $T_s = 900$ °C samples. The lower T_p in these samples than that of the parent NSMO sample indicates the extrinsic transport behaviour originated from interfaces and grain boundary effects. As seen in the SEM morphologies of figure 2, the grain boundaries in $T_s = 1100$ °C are not clear and there is a short neck between two grains whereas for $T_s = 1300$ °C, the grain boundaries are obvious and the necks among

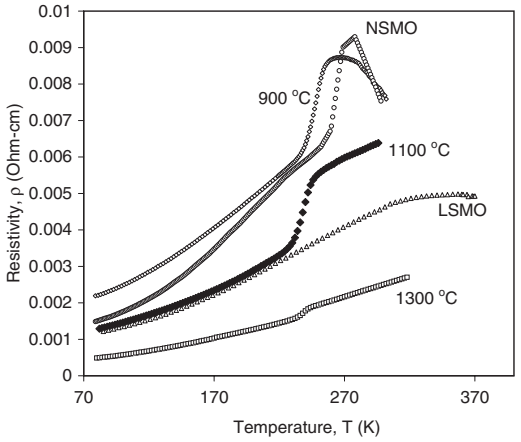

Figure 5. Temperature dependence of resistivity at zero field for LSMO, NSMO and LSMO/NSMO composites of $T_s = 900$, 1100 and 1300 °C.

grains disappear. Thus the distortion at grain boundaries which indirectly affect the inside of grains may result in the disparity between the as-observed T_p and T_c [25]. It is observed that the resistivity in the composites decreases with increasing sintering temperature. The resistivity as at room temperature was 0.0012, 0.0015, 0.0022, 0.0013 and 0.0005 Ω cm^{-1} for LSMO, NSMO, LSMO/NSMO composites at $T_s = 900$, 1100 and 1300 °C, respectively. Composites sintered at $T_s = 900$ °C have the highest resistivity among the three composites due to the enhanced spin dependent interfacial disorder created at the neighbouring grain boundaries, since the current flow is controlled by the relative orientation θ_{ij} of the magnetization of the adjacent neighbours. Thus, the distorted or bent Mn–O–Mn path and the misaligned magnetic spins decrease the conductivity in the composite by hindering the tunnelling of electrons from one place to another. The applied magnetic field of 10 kOe polarizes parts of the disordered Mn spins inside the coupling layers along the field direction. Therefore, it has the highest MR among the three composites. The MR_{max} for the corresponding LSMO, NSMO, LSMO/NSMO composites of $T_s = 900$, 1100 and 1300 °C are $\sim 13\%$ at the temperature where MR is maximum, $T_{max} \approx 365$ K, 34% at $T_{max} \approx 268$ K, 26% at $T_{max} \approx 260$ K, 18% at $T_{max} \approx 250$ K and 13% at $T_{max} \approx 245$ K, respectively. Interestingly, the MR near room-temperature decreases rapidly in NSMO, LSMO samples and composites at $T_s = 900$ and 1100 °C, whereas a rather constant MR was observed near room-temperature for composites at $T_s = 1300$ °C. This observation of broad MR around room-temperature can most likely be ascribed to the coexistence of multiphase in the composite of $T_s = 1300$ °C, which may be useful from a technological perspective.

4. Conclusions

In summary, the microstructure, magnetic and electrical transport properties of NSMO/LSMO composites at various sintering temperatures, T_s, have been investigated. It is shown that the sintering temperature plays an important role in affecting the microstructure and interfacial reaction at the grain boundary interfaces. Composite sintered at $T_s = 900$ °C has the highest MR among the three composites. This observation can be ascribed to the distorted or bent Mn–O–Mn path and enhanced magnetic spin disorder occurs across the neighbouring grains. The probability of electron tunnelling from one ferromagnetic grain to another ferromagnetic grain depends on the relative orientation between moments of two grains. The applied magnetic field suppresses the spin fluctuations and thus the probability that spin tunnelling across grain boundaries increases. With the coexistence of multiphase at $T_s = 1300$ °C composite, broad magnetoresistance around room-temperature is obtained. The results strongly suggest that

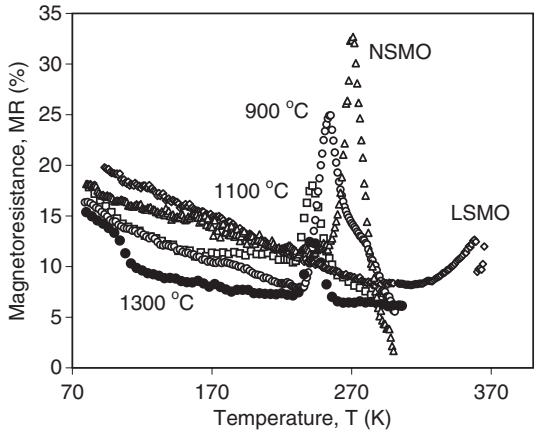

Figure 6. Temperature dependence of MR ratios for LSMO (◇), NSMO (△) and LSMO/NSMO composites at $T_s = 900\,^{\circ}C$ (○), 1100 °C (□) and 1300 °C (●).

the sintering temperature has a great effect on the properties of the grain boundary in the composites.

Acknowledgment

CYL would like to thank Mr Lim Poh Chong for his help in collecting the SEM images of the samples.

References

[1] Hwang H Y and Cheong S W 1997 *Science* **278** 1607
[2] Li X W, Gupta A, Xiao G, Qian W and Dravid V P 1998 *Appl. Phys. Lett.* **73** 3282
[3] Milner A, Gerber A, Groisman B, Karpovsky M and Gladkikh A 1996 *Phys. Rev. Lett.* **76** 475
[4] Berkowitz A E *et al* 1992 *Phys. Rev. Lett.* **68** 3745
[5] Jin S, Tiefel T H, McCormack M, Fastnact R A, Ramesh R and Chen L H 1994 *Science* **264** 413
[6] von Helmolt R, Wecker J, Holzapfel B, Schultz L and Samwer K 1993 *Phys. Rev. Lett.* **71** 2331
[7] Xiao J Q, Jiang J S and Chien C C 1992 *Phys. Rev. Lett.* **68** 3749
[8] Penney T, Shafer M W and Torrance J B 1972 *Phys. Rev.* B **5** 3669
[9] Baibich M N *et al* 1988 *Phys. Rev. Lett.* **61** 2472
[10] Parkin S S P, More N and Roche K P 1990 *Phys. Rev. Lett.* **64** 2304
[11] Levy P M 1994 *Solid State Phys.* **47** 367
[12] Levy P M and Zhang S 1995 *J. Magn. Magn. Mater.* **151** 315
[13] Hwang H Y, Cheong S W, Ong N P and Batlogg B 1996 *Phys. Rev. Lett.* **77** 2041
[14] Hotta T, Moraghebi M, Feiguinm A, Moreo A, Yunoki S and Dagotto E 2003 *Phys. Rev. Lett.* **90** 247203
[15] Coey J M D, Berkowitz A E, Balcells L I and Putris F F 1998 *Phys. Rev. Lett.* **80** 3815
[16] Issac S P, Mathur N D, Evetts J E and Blamire M G 1998 *Appl. Phys. Lett.* **72** 2038
[17] Helman J S and Abeles B 1976 *Phys. Rev. Lett.* **37** 1429
[18] Balcells L I, Carrillo A E, Martinez B and Fontcuberta J 1999 *Appl. Phys. Lett.* **74** 4014
[19] Huang Y H, Yan C H, Luo F, Song W, Wang Z M and Liao C S 2002 *Appl. Phys. Lett.* **81** 76
[20] Liu J M, Yuan G L, Sang H, Wu Z C, Chen X Y, Liu Z G, Du Y W, Huang Q and Ong C K 2001 *Appl. Phys. Lett.* **78** 1110
[21] Hueso L E, Rivas J, Rivadulla F and Lopez-Quintela M A 2001 *J. Appl. Phys.* **89** 1746
[22] Coey J M D, Viret M and vonMolnar S 1997 *Adv. Phys.* **48** 167
[23] Chang Y L, Huang Q and Ong C K 2002 *J. Appl. Phys.* **91** 789
[24] Wu W B, Wong K H, Li X G and Choy C L 2000 *J. Appl. Phys.* **87** 3006
[25] Fu Y L 2000 *Appl. Phys. Lett.* **77** 118